

# Dynamic Neural Koopman Distillation for Real-Time Robot Control Using Diffusion Models

Lei Zheng<sup>1</sup>, Peiqi Yu<sup>2</sup>, Zengqi Peng<sup>3</sup>, Changliu Liu<sup>2</sup>, and Armin Lederer<sup>1</sup>

**Abstract**—Diffusion models excel at generating diverse and multimodal trajectories for robotic planning, yet their iterative denoising process introduces latency that is incompatible with high-frequency closed-loop control. To address this problem, we propose Dynamic Neural Koopman Distillation, a framework that distills multistep diffusion inference into a single forward pass while retaining the multimodal expressivity of the teacher model. Specifically, we introduce a Factorized Dynamic Koopman layer that models the denoising process through a factorized latent transition with state-dependent modal gains. We evaluate the proposed method on standard D4RL MuJoCo locomotion benchmarks and a physical Kinova manipulator, comparing against one-step baselines. The results show that our method significantly outperforms existing one-step distillation approaches on the reported locomotion tasks, and reduces the inference latency to the millisecond regime compared with the teacher policy. Hardware experiments further demonstrate that our method enables smooth and fast closed-loop execution while maintaining task success and comparable accuracy. A project page is available at <https://fdkoopman.github.io/>.

## I. INTRODUCTION

Diffusion models have emerged as a promising approach for robotic motion generation and control [1], [2]. By shifting policy learning from deterministic state-action mappings to stochastic trajectory generation, diffusion-based policies have shown strong performance across a broad range of continuous tasks, including locomotion [3], manipulation [4], motion planning [5], and exploration [6], [7]. Unlike traditional unimodal policies, these models effectively generate diverse and context-appropriate plans, which makes them well-suited to robots operating in dynamic environments [3].

Despite this high expressivity, inference latency remains a major obstacle to deploying diffusion policies on nonlinear physical systems. During inference, a diffusion policy generates each trajectory through multiple reverse denoising steps, where a learned network sequentially transforms an initial noise sample into a task-conditioned trajectory [8], [9]. As a result, these sequential updates can lead to hundreds of

milliseconds per decision in high-dimensional control settings. This delay is incompatible with the low-latency updates required for agile closed-loop control [10].

To alleviate this latency bottleneck, researchers have explored one-step distillation frameworks, such as Consistency Models [11], [12] and Progressive Distillation [13]. These methods compress the generative process into a direct feedforward mapping and can greatly reduce inference cost. Recent studies have extended this idea to robot control [14]. Although these methods successfully reduce inference time, most one-step methods do not explicitly model the structured evolution of denoising trajectories. Consequently, they may struggle to maintain temporal consistency in physical systems, especially in tasks with strong nonlinearities or rapid changes in behavior.

Koopman operator theory provides a principled way to introduce dynamical structure into this setting by lifting nonlinear dynamics into a globally linear latent space [15], [16]. In robotics, deep Koopman models have been used to improve control and dynamics learning under limited supervision [17], [18]. However, such architectures still rely on slow and iterative upstream diffusion planners. To streamline the denoising process itself, recent efforts in image synthesis have proposed using a fixed global latent transition to compress diffusion inference into a single step [19]. Nevertheless, directly translating this static distillation framework to robot control is challenging since robotic trajectories can vary substantially across states, contact conditions, and motion regimes. A single global latent transition may therefore be too restrictive to represent denoising behavior across trajectory modes, leading to degraded control performance.

In this paper, we propose Dynamic Neural Koopman (DNK) distillation, a Koopman-inspired framework that combines the expressive planning capability of diffusion models with the speed required for real-time robot control. Using Koopman-inspired latent dynamics [18], [20], we represent the iterative denoising process of diffusion through a learned latent space equipped with a state-dependent factorized transition. This design enables millisecond-level inference latency while retaining multimodal trajectory diversity. The main contributions of this paper are summarized as follows:

- We present a one-step diffusion distillation framework for robot control by approximating the iterative reverse denoising process through one-step linear transitions in a learned latent space. This reduces inference cost relative to multistep diffusion sampling, enabling high-frequency closed-loop control for nonlinear robotic systems.
- We introduce the Factorized Dynamic Koopman (FDK) layer that represents the latent linear transition via a

<sup>1</sup>Lei Zheng and Armin Lederer are with the Department of Electrical and Computer Engineering, National University of Singapore, Singapore (e-mail: zack.zheng@nus.edu.sg; armin.lederer@nus.edu.sg).

<sup>2</sup>Peiqi Yu and Changliu Liu are with the Department of Electrical and Computer Engineering, Carnegie Mellon University, USA (e-mail: peiqiyu@andrew.cmu.edu; cliu6@andrew.cmu.edu).

<sup>3</sup>Zengqi Peng is with the Robotics and Autonomous Systems Thrust, The Hong Kong University of Science and Technology, Hong Kong SAR, China (e-mail: zpeng940@connect.ust.hk).

Corresponding author: Lei Zheng (zack.zheng@nus.edu.sg).

This work has been submitted to the IEEE for possible publication. Copyright may be transferred without notice, after which this version may no longer be accessible.

product of learned matrices and state-dependent modal gains. Compared with a fixed global latent transition [19], the FDK layer provides a more flexible parameterization of denoising dynamics, with modal-gain and inverse-consistency regularization to improve conditioning and support multimodal candidate generation.

- We evaluate the proposed method on standard D4RL MuJoCo locomotion benchmarks and a physical Kinova Gen3 manipulator. Compared with existing one-step distillation baselines, our approach achieves higher returns while considerably reducing inference latency. Hardware experiments show that the distilled policy enables faster online execution, shorter task completion time, and successful obstacle-aware reconfiguration under receding-horizon control.

## II. RELATED WORK

### A. Diffusion Models for Robot Control

Recent work has increasingly applied diffusion models to robot control, where actions or trajectories are generated by sampling from a conditional distribution rather than as a single deterministic output [1], [9]. This property makes them well-suited to robotic tasks with multimodal futures, long horizons, and ambiguity in feasible behavior. Existing studies have applied diffusion-based policies to manipulation [4], locomotion [3], motion planning [2], [21], and exploration [6], [7]. Unified software frameworks, such as CleanDiffuser, have facilitated more accessible, modular, and reproducible development of diffusion-based methods in robotics [22].

Most of these methods generate actions through iterative denoising conditioned on the current observation, task specification, or visual context. While this procedure yields expressive policies, it also entails substantial inference latency because multiple denoising steps are required before an action is produced. Such latency is manageable in offline planning, but it becomes a major limitation in closed-loop robot control, where actions must be updated at high frequency and with low delay [1]. This motivates the development of faster diffusion-based policies that remain suitable for closed-loop control.

### B. Acceleration and Distillation of Diffusion Models

Prior work on accelerating inference for diffusion models can be broadly grouped into two directions: fast samplers and distillation-based generators [14], [19]. Fast samplers reduce the number of denoising evaluations while retaining the original diffusion model. Representative examples include Denoising Diffusion Implicit Models (DDIM) [23], DPM-Solver [24], and EDM-style fast-sampling formulations [25]. These methods improve efficiency, but they remain iterative and may be too slow for high-frequency closed-loop control.

Distillation-based methods instead train a student model to reproduce the teacher with fewer denoising steps, or in a single forward pass. Progressive Distillation [13] reduces the number of sampling steps through teacher-student compression, while Consistency Models support direct or near-direct generation through Consistency Training (CT) and Consistency Distillation (CD) [11], [12]. These approaches can provide greater

reductions in inference cost than sampler acceleration and are therefore attractive for real-time control. However, most approaches learn a direct mapping from noise to action or trajectory without explicitly modeling the structured reverse denoising evolution. While such mappings can be effective in less demanding settings, they may lose multimodality or produce inconsistent trajectories when the required behavior varies across states, tasks, or motion regimes, such as in agile locomotion. Several recent works have applied one-step distillation directly to robotics [14], yet they typically treat generation as a direct mapping, rather than modeling the latent evolution that connects the noisy prior to the denoised trajectory. Our work addresses this gap by introducing a structured latent transition into the one-step distillation process.

### C. Koopman-Based Models for Nonlinear Dynamics

Koopman operator theory provides a principled way to represent nonlinear dynamics through linear evolution of observables in a lifted space [15], [18]. This perspective has motivated a broad literature on data-driven prediction and control, including neural variants that jointly learn lifted representations and approximate latent dynamics [17], [26]. In robotics, Koopman-based models have been used for system identification, prediction, and feedback control, especially when nonlinear dynamics are difficult to model directly [18].

Recently, Koopman ideas have been introduced into generative modeling. The Koopman Distillation Model (KDM) shows that diffusion denoising can be compressed into a single latent linear evolution step for image generation [19]. This result suggests that Koopman-based distillation is a promising approach to fast generative inference. However, existing Koopman diffusion formulations are developed primarily for image synthesis and rely on a static global operator. In robot control, trajectories exhibit stronger state dependence, contact changes, and tighter closed-loop timing constraints. This distinction motivates our state-dependent factorized latent transition, which is better suited to the state-dependent trajectory generation required in robot control.

## III. PROBLEM STATEMENT AND PRELIMINARIES

We consider trajectory generation for high-frequency closed-loop robot control. Let  $\mathbf{s}_k \in \mathcal{S} \subseteq \mathbb{R}^n$  and  $\mathbf{a}_k \in \mathcal{A} \subseteq \mathbb{R}^n$  denote the robot state and action at the discrete time step  $k$ , respectively. Over a prediction horizon  $H$ , a future state-action trajectory  $\tau$  is defined as

$$\tau = (\mathbf{s}_1, \mathbf{a}_1, \dots, \mathbf{s}_H, \mathbf{a}_H). \quad (1)$$

At each control step, the planner models a conditional trajectory distribution  $\pi(\tau \mid \mathbf{c})$ , where  $\mathbf{c}$  denotes the information available at the current step, such as the current observation, observation history, and task specification.

Let  $T_{\text{inf}}$  denote the inference time required to generate trajectory samples, and let  $T_{\text{ctrl}}$  denote the control period of the closed-loop system. For closed-loop deployment, the generated action must be available within the control period, i.e.,  $T_{\text{inf}} \leq T_{\text{ctrl}}$ . Our goal is to learn a one-step student generator that substantially reduces  $T_{\text{inf}}$  relative to the teacher

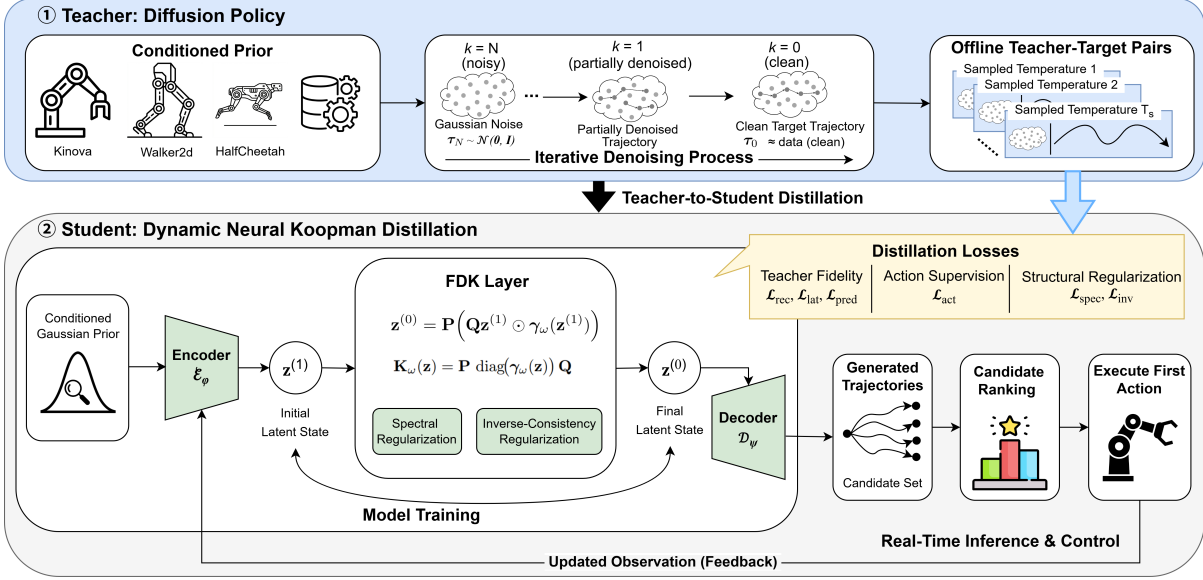


Fig. 1. Overview of the proposed DNK distillation framework. Top: a pretrained diffusion teacher generates offline teacher-target pairs from conditioned Gaussian priors. Bottom: the one-step student maps a task-conditioned Gaussian prior to a denoised trajectory through the proposed FDK latent transition. During deployment, multiple candidates are generated in parallel, ranked by an external selector, and executed in a receding-horizon control loop.

diffusion policy while preserving the conditional trajectory distribution of the teacher.

#### A. Denoising Diffusion Probabilistic Models

Denoising diffusion probabilistic models (DDPMs) learn a target distribution by reversing a Markovian noise-addition process [8], [9]. Let  $\tau_0 \sim q(\tau_0 | \mathbf{c})$  denote a denoised trajectory target conditioned on  $\mathbf{c}$ . The forward diffusion process adds Gaussian noise over  $N$  steps according to a variance schedule  $\{\beta_k\}_{k=1}^N$ , with  $\beta_k \in (0, 1)$ :

$$q(\tau_k | \tau_{k-1}) = \mathcal{N}(\tau_k; \sqrt{1 - \beta_k} \tau_{k-1}, \beta_k \mathbf{I}), \quad (2)$$

where  $\mathbf{I}$  denotes the identity matrix. Equivalently,

$$\tau_k = \sqrt{\bar{\alpha}_k} \tau_0 + \sqrt{1 - \bar{\alpha}_k} \epsilon, \quad (3)$$

where  $\bar{\alpha}_k = \prod_{i=1}^k (1 - \beta_i)$  and  $\epsilon \sim \mathcal{N}(\mathbf{0}, \mathbf{I})$ . For sufficiently large  $N$ , the terminal distribution approaches  $\mathcal{N}(\mathbf{0}, \mathbf{I})$ .

The reverse process sequentially denoises  $\tau_N$  to recover  $\tau_0$ . The resulting conditional diffusion policy can be written as

$$\pi_\theta(\tau_0 | \mathbf{c}) := \int \mathcal{N}(\tau_N; \mathbf{0}, \mathbf{I}) \prod_{k=1}^N p_\theta(\tau_{k-1} | \tau_k, \mathbf{c}) d\tau_{1:N}. \quad (4)$$

Here,  $d\tau_{1:N}$  denotes integration over the intermediate diffusion variables  $d\tau_1 \cdots d\tau_N$ . The term  $p_\theta(\tau_{k-1} | \tau_k, \mathbf{c})$  denotes the learned reverse denoising transition, defined as

$$p_\theta(\tau_{k-1} | \tau_k, \mathbf{c}) = \mathcal{N}(\tau_{k-1}; \boldsymbol{\mu}_\theta(\tau_k, \mathbf{c}, k), \boldsymbol{\Sigma}_\theta(\tau_k, \mathbf{c}, k)).$$

The denoising network  $\epsilon_\theta(\tau_k, \mathbf{c}, k)$  is trained with the standard DDPM noise-prediction objective

$$\mathcal{L}_{\text{DDPM}} = \mathbb{E}_{\tau_0, \epsilon, k} [\|\epsilon - \epsilon_\theta(\tau_k, \mathbf{c}, k)\|^2], \quad (5)$$

where  $k$  is sampled uniformly from  $\{1, \dots, N\}$ . This objective teaches the network to approximate the reverse denoising process through noise prediction.

The conditional diffusion policy in (4) reveals the main computational bottleneck: generating one trajectory sample requires  $N$  sequential network evaluations, which limits real-time deployment in high-frequency receding-horizon control.

#### B. Koopman Operator Theory and Neural Koopman Models

Koopman operator theory represents nonlinear dynamics through a linear evolution of observables in a lifted space [18], [20]. For a discrete-time nonlinear system  $\mathbf{x}^+ = \Phi(\mathbf{x})$ , where  $\mathbf{x}^+$  denotes the next state and  $\Phi$  is the nonlinear state-transition map, the Koopman operator acts on a scalar observable  $g$  as

$$(\mathcal{K}g)(\mathbf{x}) = g(\Phi(\mathbf{x})). \quad (6)$$

Although  $\Phi$  is generally nonlinear,  $\mathcal{K}$  is linear on the space of observables. In practice, this infinite-dimensional operator is approximated in a finite-dimensional lifted space [18].

Neural Koopman models parameterize the observable lifting and reconstruction maps with neural networks and aim to learn a latent space in which the dynamics are approximately linear. In this setting,

$$\mathbf{z}_k = \mathcal{E}_\phi(\tau_k), \quad \hat{\tau}_k = \mathcal{D}_\psi(\mathbf{z}_k), \quad (7)$$

where  $\mathbf{z}_k \in \mathbb{R}^L$  denotes the lifted latent representation of the trajectory variable  $\tau_k$ , with  $L$  being the latent dimension;  $\mathcal{E}_\phi$  and  $\mathcal{D}_\psi$  denote the encoder and decoder with trainable parameters  $\phi$  and  $\psi$ , respectively. Since diffusion inference proceeds from  $\tau_N$  to  $\tau_0$ , we write the latent transition in the reverse direction. The learned finite-dimensional latent evolution is then approximated by

$$\mathbf{z}_k \approx \mathbf{A} \mathbf{z}_{k+1}, \quad (8)$$

where  $\mathbf{A}$  denotes a finite-dimensional linear operator in the lifted latent space.

As outlined in [27], under suitable assumptions, finite-dimensional lifted linear representations can approximate the

original nonlinear map arbitrarily well. This motivates our use of Koopman-inspired latent modeling to approximate the evolution of trajectories along the diffusion denoising process.

#### IV. DYNAMIC NEURAL KOOPMAN DISTILLATION FRAMEWORK

This section presents the proposed DNK Distillation framework, illustrated in Fig. 1. The framework first constructs an offline teacher-target dataset by querying a pretrained DDPM teacher. It then trains a one-step student to map a task-conditioned Gaussian prior to a denoised trajectory target through a state-dependent lifted transition. The student is built on an FDK layer and trained using teacher-fidelity losses, control-oriented supervision, and structural regularization. At test time, the distilled student is deployed in a receding-horizon control loop.

##### A. Offline Teacher-Target Pair Generation

Let  $\pi_\theta$  denote the pretrained teacher diffusion policy. We construct an offline distillation dataset by sampling conditioning variables from the dataset used to train the teacher. For each context  $\mathbf{c}$ , we initialize a trajectory-shaped Gaussian noise tensor  $\tau_N = \lambda \xi$ , where  $\xi \sim \mathcal{N}(\mathbf{0}, \mathbf{I})$  and  $\lambda > 0$  is the sampling temperature, which serves as the initial variable for the reverse denoising process in (4). We then construct a conditioned prior  $\tau_{\text{prior}}^{\mathbf{c}}$  by replacing task-relevant entries of  $\tau_N$ , such as the current observation, with the corresponding values specified by  $\mathbf{c}$ . Thus,  $\lambda$  only scales the initial noise of the unfixed entries and does not modify the denoising network, diffusion schedule, or task-conditioned entries.

Following this, the teacher is queried with the conditioned prior to generate a corresponding denoised trajectory target:

$$\tilde{\tau}_0 \sim \pi_\theta(\cdot \mid \mathbf{c}; \tau_{\text{prior}}^{\mathbf{c}}), \quad (9)$$

where the semicolon indicates that the teacher reverse process is initialized from the conditioned prior  $\tau_{\text{prior}}^{\mathbf{c}}$ . The sampling temperature  $\lambda$  is used only during teacher rollout generation and is omitted from the notation for simplicity. Hence, each distillation example takes the form  $(\tau_{\text{prior}}^{\mathbf{c}}, \tilde{\tau}_0)$ , where the conditioning information  $\mathbf{c}$  is imposed through the fixed entries of  $\tau_{\text{prior}}^{\mathbf{c}}$ .

##### B. State-Dependent Lifted Dynamics via the FDK Layer

We propose an FDK layer to model one-step denoising as a state-dependent transition in a shared lifted latent space. The student first maps the conditioned prior to a latent state

$$\mathbf{z}^{(1)} = \mathcal{E}_\phi(\tau_{\text{prior}}^{\mathbf{c}}) \in \mathbb{R}^L, \quad (10)$$

where  $L$  is the lifted latent dimension. For the proposed student, the same encoder is used for both conditioned priors and denoised teacher targets, so that denoising and reconstruction are learned in the same latent space.

A static Koopman distillation model [19] applies a single global linear operator to all latent samples. This assumption is restrictive for robotic trajectory generation because the transition from a noisy prior to a denoised trajectory can vary

substantially across motion regimes and task conditions. To address this issue, we introduce an FDK layer that replaces the fixed global transition with a factorized and state-dependent latent map. Instead of predicting a full dense matrix for each sample, the FDK layer uses two learned latent maps with approximate inverse consistency together with state-dependent modal gains:

$$\mathbf{z}^{(0)} = \mathbf{P} \left( \mathbf{Q} \mathbf{z}^{(1)} \odot \gamma_\omega(\mathbf{z}^{(1)}) \right), \quad (11)$$

where  $\odot$  denotes elementwise multiplication. The matrices  $\mathbf{Q}, \mathbf{P} \in \mathbb{R}^{L \times L}$  are learned modal projection and reconstruction matrices, respectively.  $\gamma_\omega : \mathbb{R}^L \rightarrow \mathbb{R}^L$  predicts sample-dependent modal gains, where  $\omega$  denotes the parameters of the modal-gain network  $\gamma_\omega$ . Since  $\mathbf{z}^{(1)} = \mathcal{E}_\phi(\tau_{\text{prior}}^{\mathbf{c}})$ , the modal gains  $\gamma_\omega(\mathbf{z}^{(1)})$  are implicitly dependent on the condition  $\mathbf{c}$ , enabling the transition (11) to adapt to different observations and task specifications. Equivalently, the layer defines a state-dependent factorized latent transition

$$\mathbf{z}^{(0)} = \mathbf{K}_\omega(\mathbf{z}^{(1)}) \mathbf{z}^{(1)}, \quad \mathbf{K}_\omega(\mathbf{z}) = \mathbf{P} \text{diag}(\gamma_\omega(\mathbf{z})) \mathbf{Q}.$$

Compared with static Koopman distillation models [19], this yields a more flexible parameterization of denoising dynamics. Compared with a fully sample-specific dense operator, it introduces state dependence with lower parameter and computational overhead, which is important for real-time robot control.

After the FDK transition, the decoder reconstructs the predicted denoised trajectory:

$$\hat{\tau}_0 = \mathcal{D}_\psi(\mathbf{z}^{(0)}). \quad (12)$$

##### C. Training Objective

Given an offline teacher-target sample  $(\tau_{\text{prior}}^{\mathbf{c},(i)}, \tilde{\tau}_0^{(i)})$  from the dataset defined in Section IV-A, the student predicts a denoised trajectory  $\hat{\tau}_0^{(i)}$ . The training objective combines teacher-fidelity losses, control-oriented supervision, structural regularization, and teacher-quality reweighting.

1) *Teacher-Fidelity Losses*: To distill the teacher into a one-step student, we align the student with the teacher using three complementary terms: denoised-trajectory reconstruction, latent-transition consistency, and trajectory prediction:

$$\mathcal{L}_{\text{rec}} = \mathbb{E} \left[ \|\mathcal{D}_\psi(\mathcal{E}_\phi(\tilde{\tau}_0)) - \tilde{\tau}_0\|_2^2 \right], \quad (13)$$

$$\mathcal{L}_{\text{lat}} = \mathbb{E} \left[ \|\mathbf{z}^{(0)} - \text{sg}(\mathcal{E}_\phi(\tilde{\tau}_0))\|_2^2 \right], \quad (14)$$

$$\mathcal{L}_{\text{pred}} = \mathbb{E} \left[ \|\hat{\tau}_0 - \tilde{\tau}_0\|_2^2 \right]. \quad (15)$$

Here,  $\mathcal{L}_{\text{rec}}$  regularizes the encoder–decoder pair so that denoised teacher trajectories are represented in a shared latent space;  $\mathcal{L}_{\text{lat}}$  aligns the FDK-evolved latent state with the encoded teacher target, coupling the latent-state-dependent transition to the representation used for reconstruction. The stop-gradient operator  $\text{sg}(\cdot)$  blocks gradients through the encoded teacher-target branch, so  $\mathcal{E}_\phi(\tilde{\tau}_0)$  serves as a fixed latent target for the FDK-evolved state  $\mathbf{z}^{(0)}$ . This facilitates latent alignment while preserving representation learning through  $\mathcal{L}_{\text{rec}}$  and  $\mathcal{L}_{\text{pred}}$ . Finally,  $\mathcal{L}_{\text{pred}}$  directly supervises the decoded trajectory to match the teacher target.

2) *Control-Oriented Supervision*: Since only the first action is executed in a receding-horizon manner, control performance depends strongly on near-term action prediction. We therefore augment the objective with a weighted action-sequence loss defined directly on the predicted and teacher-target trajectories. Let  $\Pi_a(\boldsymbol{\tau}) = [\mathbf{a}_1^\top, \dots, \mathbf{a}_H^\top]^\top \in \mathbb{R}^{Hn}$  denote the action sequence extracted from trajectory  $\boldsymbol{\tau}$ . We define

$$\mathcal{L}_{\text{act}} = \mathbb{E} \left[ \|\Pi_a(\hat{\boldsymbol{\tau}}_0) - \Pi_a(\tilde{\boldsymbol{\tau}}_0)\|_{\mathbf{W}_a}^2 \right], \quad (16)$$

where  $\|\mathbf{x}\|_{\mathbf{W}_a}^2 = \mathbf{x}^\top \mathbf{W}_a \mathbf{x}$ . We exploit the diagonal matrix  $\mathbf{W}_a$  to assign a larger weight to the first action than to later actions, such that immediately executed control is emphasized while still enforcing consistency over the full predicted action sequence.

3) *Structural Regularization*: To regularize the factorized latent transition, we introduce two structurally motivated regularizers. The first limits excessive modal amplification:

$$\mathcal{L}_{\text{spec}} = \mathbb{E} \left[ \frac{1}{L} \sum_{\ell=1}^L \max(0, |\gamma_{\omega, \ell}(\mathbf{z})| - 1) \right], \quad (17)$$

where  $\gamma_{\omega, \ell}(\mathbf{z})$  denotes the  $\ell$ -th state-dependent coefficient produced by the FDK modulation network. This term discourages excessive amplification in the lifted transition and facilitates stable training. The second regularizer encourages the two latent maps to remain approximately inverse:

$$\mathcal{L}_{\text{inv}} = \|\mathbf{PQ} - \mathbf{I}\|_F^2, \quad (18)$$

where  $\|\cdot\|_F$  denotes the Frobenius norm. This term encourages the modal projection and reconstruction matrices to behave as approximate inverses and improve the conditioning of the factorized latent transition.

4) *Total Objective*: To emphasize higher-quality teacher targets during training, we use the cumulative-return classifier from the teacher diffusion pipeline to assign each teacher-generated trajectory a scalar quality score  $r^{(i)}$ . This score is mapped to a sample weight  $w^{(i)} \in [1, 1 + \beta]$  by quantile normalization, with  $\beta = 1.0$  in this study.

Combining the reweighted terms with the structural regularizers, the total training objective is

$$\begin{aligned} \mathcal{L} = & \alpha_{\text{rec}} \mathcal{L}_{\text{rec}} + \alpha_{\text{lat}} \mathcal{L}_{\text{lat}} + \alpha_{\text{pred}} \mathcal{L}_{\text{pred}} \\ & + \alpha_{\text{act}} \mathcal{L}_{\text{act}} + \alpha_{\text{spec}} \mathcal{L}_{\text{spec}} + \alpha_{\text{inv}} \mathcal{L}_{\text{inv}}, \end{aligned} \quad (19)$$

where  $\alpha_{\text{rec}}$ ,  $\alpha_{\text{lat}}$ ,  $\alpha_{\text{pred}}$ ,  $\alpha_{\text{act}}$ ,  $\alpha_{\text{spec}}$ , and  $\alpha_{\text{inv}}$  are the corresponding loss weights. The data-fitting losses in (13), (14), (15), and (16) are computed using the per-sample weights  $w^{(i)}$ , whereas the structural regularizers in (17) and (18) are not sample-weighted.

#### D. Inference: Batched One-Step Receding-Horizon Control

After training, the distilled student is deployed in a receding-horizon control manner, as illustrated in Fig. 1. At each control step, a conditioned Gaussian prior trajectory  $\boldsymbol{\tau}_{\text{prior}}$  is constructed by sampling Gaussian noise and encoding current task-relevant context into the prior representation.

We draw  $N_{\text{cand}}$  independent noise seeds and evaluate the student on the resulting batch of conditioned priors. This

yields a set of candidate trajectories in parallel. These candidates are then ranked by an external selector, such as an Implicit Q-Learning (IQL) critic with argmax selection [28] or a teacher-side classifier [22], which assigns each candidate a task-dependent control score. The controller executes the first action of the highest-scoring candidate and replans at the next control step using updated observations. This inference scheme separates multimodal candidate generation from control-oriented candidate selection, allowing the student to retain distributional diversity while the selector enforces action quality at execution time [29].

## V. EXPERIMENTAL RESULTS

In this section, we evaluate the proposed DNK distillation framework on D4RL MuJoCo locomotion benchmarks [30] and a real-world Kinova Gen3 obstacle-aware control task.

### A. Simulation Setup

**Benchmarks and Teacher**: We evaluate the proposed method on two standard D4RL MuJoCo locomotion tasks, `halfcheetah-medium-expert-v2` and `walker2d-medium-expert-v2`, with the observation dimension of 17 and the action dimension of 6. Following the CleanDiffuser setting [22], we train a trajectory diffusion teacher together with a cumulative-return classifier for classifier guidance during sampling and candidate ranking. The planning horizon is set to 4 for HalfCheetah and 32 for Walker2d, following the benchmark-specific setting used in the CleanDiffuser [22] pipeline. The teacher uses 20 reverse diffusion steps during inference.

To construct the offline distillation dataset, we generate 500,000 teacher-target pairs  $(\boldsymbol{\tau}_{\text{prior}}, \tilde{\boldsymbol{\tau}}_0)$  for each task. The teacher is sampled with sampling temperatures  $\lambda \in \{0.3, 0.5, 0.7\}$  and probabilities  $\{0.25, 0.5, 0.25\}$ , respectively, which increases the variation in the distilled supervision. The weighting coefficients  $\alpha_{\text{pred}}$ ,  $\alpha_{\text{rec}}$ ,  $\alpha_{\text{lat}}$ ,  $\alpha_{\text{act}}$ ,  $\alpha_{\text{spec}}$ , and  $\alpha_{\text{inv}}$  are set to 1.0, 0.8, 0.2, 1.0, 0.01, and 1.0, respectively. For the weighted action loss, we use  $\mathbf{W}_a = \text{diag}(w_1 \mathbf{I}_n, w_2 \mathbf{I}_n, \dots, w_H \mathbf{I}_n)$ , with  $w_1 = 1.5$  and  $w_k = 0.6$  for  $k = 2, \dots, H$ .

**Student Models and Baselines**: We compare the proposed method against three groups of baselines. First, we include the diffusion teacher as a high-quality but computationally expensive reference. Second, we compare with two static Koopman baselines, KDM and KDM-F [19], which use the same offline distillation setting but different latent-transition parameterizations. Third, we compare with one-step action-generation baselines based on the consistency-policy framework, including CT [11] and CD [12]. For the teacher and the one-step action-generation baselines, we use the public CleanDiffuser implementation<sup>1</sup>.

All Koopman-family students, including our dynamic model, KDM, and KDM-F, are trained on the same teacher-generated offline distillation dataset. To ensure a fair comparison, these models use a matched training configuration

<sup>1</sup><https://github.com/CleanDiffuserTeam/CleanDiffuser>

TABLE I  
QUANTITATIVE COMPARISON ON D4RL MUJoCo LOCOMOTION BENCHMARKS. WE COMPARE THE PROPOSED DNK DISTILLATION METHOD WITH ONE-STEP BASELINES AND THE MULTISTEP DIFFUSION TEACHER. RETURN AND LATENCY ARE REPORTED AS MEAN  $\pm$  STD OVER FIVE SEEDS. BOLD ENTRIES DENOTE THE BEST RESULT.

Task	Method	Return $\uparrow$	Latency (ms) $\downarrow$	$\sigma_{ep}$ $\downarrow$	Worst-case $\uparrow$
Walker2d	Teacher [22]	1.0295 $\pm$ 0.0051	301.22 $\pm$ 2.41	0.0193	0.9759
	CD [11]	0.6144 $\pm$ 0.0176	1.09 $\pm$ 2.33	0.0577	0.4808
	CT [12]	0.4404 $\pm$ 0.0096	1.09 $\pm$ 2.37	0.0659	0.2591
	KDM [19]	0.6057 $\pm$ 0.0156	<b>0.35 <math>\pm</math> 0.04</b>	0.0333	0.5925
	KDM-F [19]	0.3386 $\pm$ 0.0070	0.87 $\pm$ 0.03	0.0380	0.3267
	<b>Ours</b>	<b>1.0973 <math>\pm</math> 0.0002</b>	1.75 $\pm$ 0.36	<b>0.0004</b>	<b>1.0963</b>
	Ours (classifier)	1.0285 $\pm$ 0.0022	4.57 $\pm$ 0.87	0.0242	0.9677
HalfCheetah	Teacher [22]	0.8518 $\pm$ 0.0032	116.51 $\pm$ 2.39	0.0114	0.8229
	CD [11]	0.4027 $\pm$ 0.0109	1.08 $\pm$ 2.32	0.0277	0.3217
	CT [12]	0.4089 $\pm$ 0.0047	1.08 $\pm$ 2.31	0.0198	0.3663
	KDM [19]	0.6618 $\pm$ 0.0045	<b>0.34 <math>\pm</math> 0.03</b>	0.0349	0.6571
	KDM-F [19]	0.4852 $\pm$ 0.0098	0.86 $\pm$ 0.03	0.0216	0.4659
	<b>Ours</b>	<b>0.8885 <math>\pm</math> 0.0042</b>	0.82 $\pm$ 0.47	0.0134	<b>0.8488</b>
	Ours (classifier)	0.8599 $\pm$ 0.0010	1.83 $\pm$ 0.80	<b>0.0081</b>	0.8417

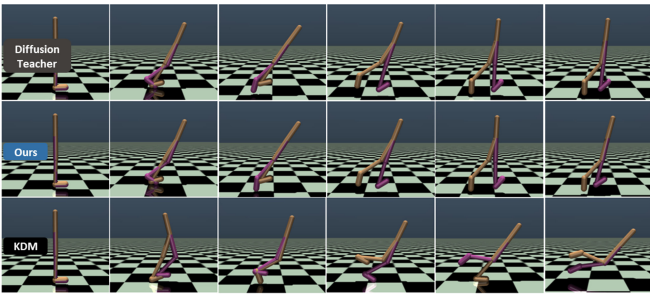


Fig. 2. Consecutive frames from rollouts of different policies on the Walker2d task. The static KDM policy [19] fails to produce a stable gait in this example. In contrast, the diffusion teacher and the proposed DNK distillation method generate coordinated forward motion.

with latent dimension  $L = 512$ , batch size 64, learning rate  $3 \times 10^{-4}$ , and 200 training epochs.

**Evaluation Protocol:** For the main one-step comparison, all student methods are evaluated under the same protocol: 64 candidate trajectories, IQL-based candidate scoring, and argmax selection. Each method is evaluated over five seeds with 500 rollouts per seed with a maximum rollout length of 1000 steps. The diffusion teacher is evaluated separately under its native protocol, namely 20-step reverse diffusion with classifier-based re-ranking, and is reported as a reference rather than as a latency-matched one-step baseline. To study the effect of the scoring mechanism, we additionally report *Ours (classifier)*, which replaces the IQL selector with the teacher-side classifier.

We report normalized D4RL return (mean  $\pm$  std over 5 seeds), worst-case return, and inference latency. Worst-case return is the minimum across seeds of the per-run episode-mean return. Latency is measured as the policy decision time per control step on an NVIDIA RTX 5090 GPU with CUDA synchronization enabled. We also report intra-run variability  $\sigma_{ep}$ , defined as the standard deviation of per-episode returns within each run, averaged over seeds.

## B. Simulation Results

**Overall Control Performance:** Table I summarizes the quantitative results. Our method achieves the highest nor-

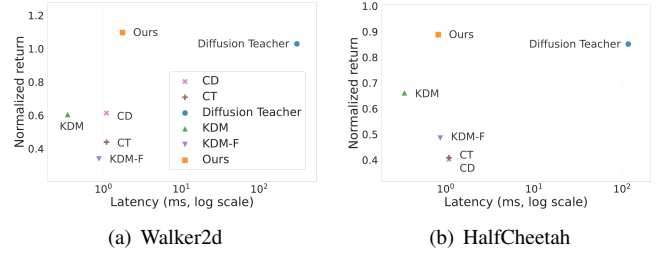


Fig. 3. Latency–performance trade-off on D4RL MuJoCo tasks. Each point denotes one method. The x-axis shows mean decision latency in milliseconds on a log scale, and the y-axis shows normalized return.

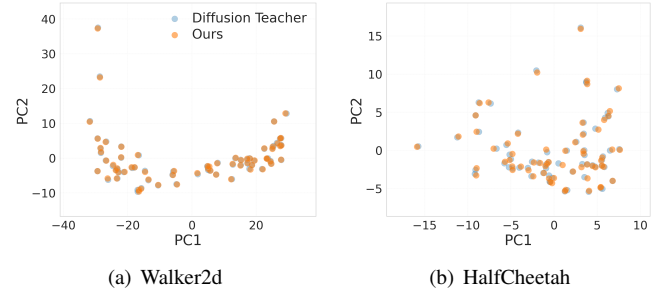


Fig. 4. Principal Component Analysis (PCA) projection of 64 candidate trajectories from the same initial state for the diffusion teacher and the proposed method. The proposed method produces candidate trajectories that occupy a broad region in the PCA projection and visually overlap with teacher-generated candidates. The percentages indicate the variance explained by the first two principal components: Walker2d (PC1/PC2 = 60.44%/7.04%), HalfCheetah (PC1/PC2 = 31.15%/19.16%).

malized returns on both tasks, reaching  $0.8885 \pm 0.0042$  on HalfCheetah and  $1.0973 \pm 0.0002$  on Walker2d. It also yields the highest worst-case returns, suggesting improved performance consistency across seeds. Notably, the proposed one-step student attains comparable to or higher returns than those of the multistep diffusion teacher reference under the reported protocols. We attribute this improvement partly to the teacher-weighted offline distillation strategy, which emphasizes higher-scoring teacher trajectories during training.

In contrast, the consistency-based baselines CD and CT remain well below the teacher in both environments. The static Koopman baselines KDM and KDM-F also perform substantially worse than both the teacher and the proposed method, with larger variance across seeds. As illustrated in Fig. 2, the static KDM policy on Walker2d fails to produce a stable forward gait in a representative rollout. This behavior further suggests that a single global latent transition may be too rigid to capture the state-dependent denoising behavior associated with physical-control trajectories.

The comparison between *Ours* and *Ours (classifier)* further shows that both selection mechanisms produce strong policies, while IQL-based scoring yields slightly higher returns overall. This is consistent with the receding-horizon setting, in which only the first action is executed before replanning. In this setting, a critic-based selector that emphasizes immediate action quality may be better matched to control execution than a trajectory-level classifier reused from the teacher pipeline.

**Real-Time Performance and the Pareto Frontier:** Compared with the diffusion teacher, the proposed method substan-

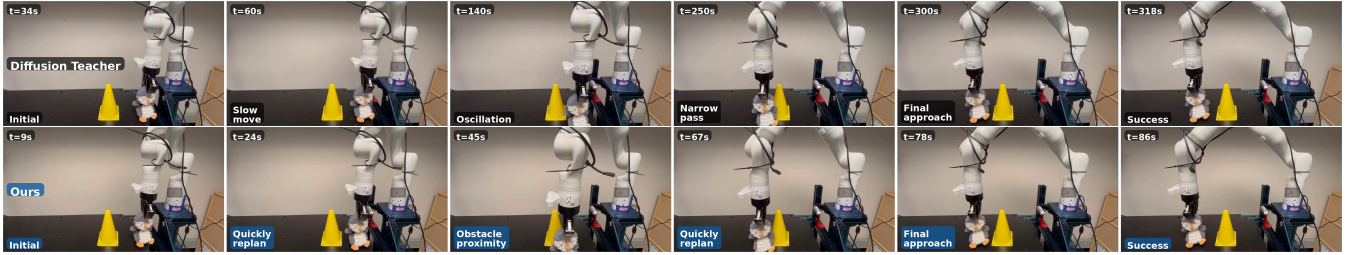


Fig. 5. Consecutive frames of the Kinova in the real-world setup. The teacher policy shows slower corrective motion near obstacles, whereas the proposed student replans more promptly and traverses the narrow region with smoother obstacle-avoidance behavior and shorter goal-reaching time.

tially reduces decision latency. The diffusion teacher requires 20 inference steps, leading to decision times of 116.51 ms and 301.22 ms on HalfCheetah and Walker2d, respectively. In contrast, our method uses a one-step student and reduces the latency to 0.82 ms and 1.75 ms, respectively, as summarized in Table I. These reductions correspond to approximately  $142\times$  and  $172\times$  speedups over the teacher on HalfCheetah and Walker2d, respectively.

Figure 3 further illustrates the latency–return trade-off across policy families. Our method achieves a favorable latency–return trade-off, maintaining teacher-level return at low latency. This operating point is desirable for high-frequency closed-loop control, where multistep diffusion policies can be too slow for practical deployment.

**Variability and Multimodal Candidate Generation:** The proposed latent transition uses spectral and inverse-consistency regularization to discourage excessive amplification in the lifted dynamics and improve conditioning during training. Empirically, this regularization is reflected in the low intra-run variability reported in Table I. In particular, on Walker2d, our method achieves the lowest intra-run variability ( $\sigma_{ep} = 0.0004$ ) among all one-step baselines.

This improved stability is also reflected in worst-case performance. Our method achieves the highest worst-case returns on both benchmarks, indicating that the learned policy remains reliable even under unfavorable runs. Moreover, Fig. 4 shows that the candidate trajectories generated by our method occupy a broad, teacher-aligned region in the PCA projection. Together with the return and variability results in Table I, these observations suggest performance consistency and better qualitative alignment with the teacher’s candidate distribution.

### C. Real-World Experiments

**Hardware Platform and Setup:** To evaluate the proposed method in a real robotic setting, we consider an obstacle-aware reconfiguration task on a Kinova Gen3 manipulator, as shown in Fig. 5. The robot moves from an initial configuration to a goal configuration while avoiding static obstacles in the workspace. During execution, the planner operates online in a receding-horizon manner using the current robot state, goal specification, and obstacle representation.

The training data are generated offline using a custom-built B-spline planner over randomized start states, goal states, and obstacle layouts. The resulting collision-aware trajectories are used to train a trajectory diffusion teacher. The proposed student is then trained to distill the teacher policy under

TABLE II  
HARDWARE COMPARISON ON THE KINOVA RECONFIGURATION TASK OVER 50 TRIALS. VALUES ARE REPORTED AS MEAN  $\pm$  STD.

Metric	Diffusion Teacher	Ours
Mean inference latency (ms) $\downarrow$	151.00 $\pm$ 3.73	<b>4.08 <math>\pm</math> 0.20</b>
P95 inference latency (ms) $\downarrow$	158.27 $\pm$ 3.78	<b>4.73 <math>\pm</math> 0.23</b>
Completion time (s) $\downarrow$	314.95 $\pm$ 3.54	<b>85.43 <math>\pm</math> 2.53</b>
Terminal error (mm) $\downarrow$	<b>3.09 <math>\pm</math> 1.42</b>	3.46 $\pm$ 1.75
Minimum clearance (mm) $\uparrow$	46.29 $\pm$ 12.91	<b>48.95 <math>\pm</math> 12.12</b>
Success rate (%) $\uparrow$	<b>100.0</b>	<b>100.0</b>

the same task conditioning, including the robot state, goal specification, and obstacle representation.

The teacher and student are evaluated with the same task specification, replanning pipeline, and low-level controller. We use the Kinova Gen3 internal Cartesian position controller, with target commands published at 20 Hz. During online planning, the teacher uses 30 reverse diffusion steps, the prediction horizon is set to 32 steps, and 64 candidates are ranked by a geometry-based score that rewards obstacle clearance and penalizes control effort. The first action of the highest-scoring candidate is executed. Success is defined as reaching the goal within  $r_{goal} = 5$  mm without collision or timeout. Each method is evaluated over 50 hardware trials using inference latency, task completion time, terminal error, minimum obstacle clearance, and success rate. We report both mean and 95th-percentile inference latency to quantify average and tail computation time. Terminal error is the final end-effector distance to the goal, while minimum clearance is the closest distance between the end-effector trajectory and the obstacle surface during execution. All online inference is evaluated on a Titan workstation running Ubuntu 20.04 with two NVIDIA TITAN RTX GPUs, each with 24 GB of VRAM; this specification is reported for reproducibility and does not imply a deployment requirement.

**Results:** Table II reports the hardware results on the Kinova reconfiguration task. The proposed one-step student reduces the mean inference latency from 151.00 ms to 4.08 ms, corresponding to an approximately  $37.0\times$  reduction relative to the diffusion teacher. Its P95 inference latency is 4.73 ms, which remains well below the 50 ms command period. In contrast, the teacher exceeds this period and therefore produces delayed commands during closed-loop execution. This latency reduction is reflected in the task completion time, which decreases from 314.95 s to 85.43 s.

The reduction in latency does not degrade task accuracy or obstacle clearance. Both methods achieve a 100.0% success

rate over 50 hardware trials. The terminal error remains comparable to the teacher, with  $3.46 \pm 1.75$  mm for our method and  $3.09 \pm 1.42$  mm for the teacher. Additionally, the proposed method achieves a slightly larger mean obstacle clearance, indicating that the faster inference does not compromise obstacle-avoidance behavior in this task.

Figure 5 further illustrates the difference in execution behavior. The diffusion teacher exhibits slower corrective motion and visible hesitation near the obstacle, whereas the proposed student replans more promptly and produces smoother obstacle-avoidance behavior before reaching the goal. These observations are consistent with the measured completion times and indicate that the distilled student is better suited to closed-loop real-time control on the physical system.

These results support the empirical effectiveness of factorized Koopman distillation for real-time hardware deployment.

## VI. CONCLUSION AND FUTURE WORK

This work presents a DNK distillation framework that distills a multistep diffusion policy into a one-step policy through an FDK layer with spectral and inverse-consistency regularization. The method achieves strong one-step performance on D4RL locomotion benchmarks and on a Kinova manipulator task, while substantially reducing inference latency relative to the diffusion teacher. Hardware experiments further demonstrate fast online execution and successful obstacle-aware reconfiguration under receding-horizon control. Despite these results, the current study does not explicitly address safety-critical constraints or richer interaction settings. Future work will extend the framework to safety-critical control and more complex unstructured environments, including human-robot interaction scenarios.

## REFERENCES

- [1] J. Urain, A. Mandlekar, Y. Du, N. Muhammad, D. Xu, K. Fragkiadaki, G. Chalvatzaki, J. Peters *et al.*, “A survey on deep generative models for robot learning from multimodal demonstrations,” *IEEE Transactions on Robotics*, vol. 42, pp. 60–79, 2025.
- [2] M. Peng, K. Chen, X. Guo, Q. Zhang, H. Zhong, M. Zhu, and H. Yang, “Diffusion models for intelligent transportation systems: A survey,” *IEEE Transactions on Intelligent Transportation Systems*, vol. 26, no. 12, pp. 21 526–21 543, 2025.
- [3] C. Pan, Z. Yi, G. Shi, and G. Qu, “Model-based diffusion for trajectory optimization,” *Advances in Neural Information Processing Systems*, vol. 37, pp. 57 914–57 943, 2024.
- [4] C. Chi, Z. Xu, S. Feng, E. Cousineau, Y. Du, B. Burchfiel, R. Tedrake, and S. Song, “Diffusion policy: Visuomotor policy learning via action diffusion,” *The International Journal of Robotics Research*, vol. 44, no. 10-11, pp. 1684–1704, 2025.
- [5] R. Yang, L. Zheng, R. Yao, and J. Ma, “DualShield: Safe model predictive diffusion via reachability analysis for interactive autonomous driving,” *arXiv preprint arXiv:2601.15729*, 2026.
- [6] S. Samavi, A. Lem, F. Sato, S. Chen, Q. Gu, K. Yano, A. P. Schoellig, and F. Shkurti, “SICNav-Diffusion: Safe and interactive crowd navigation with diffusion trajectory predictions,” *IEEE Robotics and Automation Letters*, vol. 10, no. 9, pp. 8738–8745, 2025.
- [7] Y. Cao, J. Lew, J. Liang, J. Cheng, and G. Sartoretti, “DARE: Diffusion policy for autonomous robot exploration,” in *IEEE International Conference on Robotics and Automation*, 2025, pp. 11 987–11 993.
- [8] Y. Song, J. Sohl-Dickstein, D. P. Kingma, A. Kumar, S. Ermon, and B. Poole, “Score-based generative modeling through stochastic differential equations,” in *International Conference on Learning Representations*, 2021.
- [9] J. Ho, A. Jain, and P. Abbeel, “Denoising diffusion probabilistic models,” *Advances in Neural Information Processing Systems*, vol. 33, pp. 6840–6851, 2020.
- [10] J. Hwangbo, J. Lee, A. Dosovitskiy, D. Bellicoso, V. Tsounis, V. Koltun, and M. Hutter, “Learning agile and dynamic motor skills for legged robots,” *Science Robotics*, vol. 4, no. 26, p. eaa5872, 2019.
- [11] Y. Song, P. Dhariwal, M. Chen, and I. Sutskever, “Consistency models,” in *International Conference on Machine Learning*, 2023, pp. 32 211–32 252.
- [12] Y. Song and P. Dhariwal, “Improved techniques for training consistency models,” in *International Conference on Learning Representations*, 2024.
- [13] T. Salimans and J. Ho, “Progressive distillation for fast sampling of diffusion models,” in *International Conference on Learning Representations*, 2022.
- [14] Z. Wang, M. Li, A. Mandlekar, Z. Xu, J. Fan, Y. Narang, L. Fan, Y. Zhu, Y. Balaji, M. Zhou, M.-Y. Liu, and Y. Zeng, “One-step diffusion policy: Fast visuomotor policies via diffusion distillation,” in *International Conference on Machine Learning*, 2025.
- [15] P. Bevanda, S. Sosnowski, and S. Hirche, “Koopman operator dynamical models: Learning, analysis and control,” *Annual Reviews in Control*, vol. 52, pp. 197–212, 2021.
- [16] L. Shi, M. Haseli, G. Mamakoukas, D. Bruder, I. Abraham, T. Murphey, J. Cortés, and K. Karydis, “Koopman operators in robot learning,” *IEEE Transactions on Robotics*, 2026.
- [17] J. Bi, K. Lim, K. Chen, Y. Huang, and H. Soh, “Imitation learning with limited actions via diffusion planners and deep Koopman controllers,” in *IEEE International Conference on Robotics and Automation*, 2025, pp. 4861–4868.
- [18] R. Strässer, K. Worthmann, I. Mezić, J. Berberich, M. Schaller, and F. Allgöwer, “An overview of Koopman-based control: From error bounds to closed-loop guarantees,” *Annual Reviews in Control*, vol. 61, p. 101035, 2026.
- [19] N. Berman, I. Naiman, M. Eliasof, H. Zisling, and O. Azencot, “One-Step Offline Distillation of Diffusion-based Models via Koopman Modeling,” in *Advances in Neural Information Processing Systems*, 2025.
- [20] I. Mezić, “Spectral properties of dynamical systems, model reduction and decompositions,” *Nonlinear Dynamics*, vol. 41, no. 1, pp. 309–325, 2005.
- [21] R. Zhong, R. Yao, P. Liu, X. Chen, R. Yang, and J. Ma, “CoPlanner: An interactive motion planner with contingency-aware diffusion for autonomous driving,” in *IEEE International Conference on Robotics and Automation*, 2026.
- [22] Z. Dong, Y. Yuan, J. Hao, F. Ni, Y. Ma, P. Li, and Y. Zheng, “Cleandiffuser: An easy-to-use modularized library for diffusion models in decision making,” *Advances in Neural Information Processing Systems*, vol. 37, pp. 86 899–86 926, 2024.
- [23] J. Song, C. Meng, and S. Ermon, “Denoising diffusion implicit models,” in *International Conference on Learning Representations*, 2021.
- [24] C. Lu, Y. Zhou, F. Bao, J. Chen, C. Li, and J. Zhu, “DPM-Solver: A fast ODE solver for diffusion probabilistic model sampling in around 10 steps,” *Advances in Neural Information Processing Systems*, vol. 35, pp. 5775–5787, 2022.
- [25] T. Karras, M. Aittala, T. Aila, and S. Laine, “Elucidating the design space of diffusion-based generative models,” *Advances in Neural Information Processing Systems*, vol. 35, pp. 26 565–26 577, 2022.
- [26] F. Li, A. Abuduweili, Y. Sun, R. Chen, W. Zhao, and C. Liu, “Continual learning and lifting of Koopman dynamics for linear control of legged robots,” in *Proceedings of the Annual Learning for Dynamics & Control Conference*, 2025, p. 136–148.
- [27] P. Bevanda, M. Beier, A. Lederer, S. Sosnowski, E. Hüllermeier, and S. Hirche, “Koopman kernel regression,” *Advances in Neural Information Processing Systems*, vol. 36, pp. 16 207–16 221, 2023.
- [28] I. Kostrikov, A. Nair, and S. Levine, “Offline reinforcement learning with implicit Q-learning,” in *International Conference on Learning Representations*, 2022.
- [29] T.-Y. Huang, A. Lederer, N. Hoischen, J. Brudigam, X. Xiao, S. Sosnowski, and S. Hirche, “Toward near-globally optimal nonlinear model predictive control via diffusion models,” in *Proceedings of the Annual Learning for Dynamics & Control Conference*, ser. Proceedings of Machine Learning Research, vol. 283, 04–06 Jun 2025, pp. 777–790.
- [30] J. Fu, A. Kumar, O. Nachum, G. Tucker, and S. Levine, “D4RL: Datasets for deep data-driven reinforcement learning,” *arXiv preprint arXiv:2004.07219*, 2020.